1 **Retrieval of Snow Properties for Ku- and Ka-band Dual-Frequency Radar**

2

3

4

5 Liang Liao[1], Robert Meneghini[2], Ali Tokay[3] and Larry F. Bliven[4]

6

7 [1] Goddard Earth Science Technology & Research, Morgan State University, MD

8 [2] NASA Goddard Space Flight Center, Greenbelt, MD

9 [3] University of Maryland Baltimore County/JCET, MD

10 [4] NASA Wallops Flight Facility, VA

11

12

13 Submitted to

14 Journal of Applied Meteorology and Climatology
15

16

17

18 Corresponding author information:
19
20 Dr. Liang Liao
21 Goddard Earth Sciences Technology and Research
22 Morgan State University
23 Code 612
24 NASA/Goddard Space Flight Center
25 Greenbelt, MD 20771
26
27 301-614-5718 (phone)
28 301-614-5492 (fax)
29 Email: Liang.Liao-1@ nasa.gov
30

Abstract

The focus of this study is on the estimation of snow microphysical properties and the associated bulk parameters such as snow water content and water equivalent snowfall rate for Ku- and Ka-band dual-frequency radar. This is done by exploring a suitable scattering model and the proper particle size distribution (PSD) assumption that accurately represent, in the electromagnetic domain, the micro/macro-physical properties of snow. The scattering databases computed from simulated aggregates for small to moderate particle sizes are combined with a simple scattering model for large particle sizes to characterize snow scattering properties over the full range of particle sizes. With use of the single scattering results, the snow retrieval look-up tables can be formed in a way that directly links the Ku- and Ka-band radar reflectivities to snow water content and equivalent snowfall rate without use of the derived PSD parameters. A sensitivity study of the retrieval results to the PSD and scattering models is performed to better understand the dual-wavelength retrieval uncertainties. To aid in the development of the Ku- and Ka-band dual-wavelength radar technique and to further evaluate its performance, self-consistency tests are conducted using measurements of the snow PSD and fall velocity acquired from the Snow Video Imager/Particle Image Probe (SVI/PIP) during the winter of 2014 in the NASA Wallops flight facility site in Wallops Island, Virginia.

1   Introduction

The Global Precipitation Measurement (GPM) core satellite, a joint Earth-observing mission between the National Aeronautics and Space Administration (NASA) and the Japan Aerospace Exploration Agency (JAXA), was successfully launched into orbit on 27 February of 2014 from Japan (Hou et al. 2008 and 2014). One of the goals of the Dual-frequency Precipitation Radar (DPR) aboard the GPM satellite is to provide measurements and estimates of snow precipitation rate and water content for mid- and high-latitude regions. This is usually done by estimating parameters of snow particle size distribution (PSD) that are often modeled by an analytical function, such as the exponential, gamma or lognormal distribution, with two or three unknown parameters (Gorgucci et al. 2000 and 2002; Bringi et al. 2002). The inability of the modeled PSD to represent actual snow spectra and to characterize their intrinsic variations in time and space can lead to errors in the estimates of precipitation rate obtained from the DPR. Additionally, uncertainties associated with scattering computations of snow aggregates also affect the accuracy of the dual-wavelength radar retrieval of snow arising from the complex shape and structure of snow aggregates and the corresponding variability in the scattering parameters. Therefore, understanding the uncertainties in snow precipitation estimation that depend on PSD parameterizations and scattering models of individual particles is important in evaluating the overall performance of DPR retrieval algorithms and in gaining insight into ways to improve the algorithms.

Several studies have been carried out using dual-frequency radar for the retrieval of precipitating ice/snow parameters from the ground (Matrosov 1998; Szyrmer and Zawadzki 2014) and from airborne radar measurements (Liao et al. 2005, 2008; Heymsfield et al. 2005; Wang et al. 2005;

73   Matrosov et al. 2005). Although various combinations of frequencies were used in these studies,

74   a common feature is that at least one of the radar frequencies operates in the non-Rayleigh

75   regime to ensure a measurable difference in the reflectivities. It is this differential reflectivity

76   that can be related to a characteristic size parameter of the snow particle distribution.   Because

77   of uncertainties in the snow microphysics arising from the natural variability of the particle

78   density, shape, and orientation and also because of uncertainties associated with the particle

79   backscattering cross section and terminal fall velocity as well as the natural variability in PSDs,

80   it is important to assess the errors in the model and their impacts on the retrievals.

81

82   The emphasis of this study is on the estimation of snow microphysical properties and the

83   associated bulk parameters such as snow water content and water equivalent snowfall rate. As

84   indicated earlier, one of the challenges in the radar retrieval of snow is to characterize the

85   variability of the snow PSD and to efficiently compute scattering properties of the snowflakes

86   over the full range of sizes. The aim of our study is to explore a suitable scattering model and an

87   appropriate PSD that accurately represents, in the electromagnetic domain, the micro/macro-

88   physical properties of snow.

89

90   Although several scattering databases are available, which provide the scattering properties of

91   snow aggregates (Liu 2004 and 2008; Nowell et al. 2013; Kuo et al. 2016), they are often limited

92   to small-to-moderate particle sizes for a limited set of frequencies. These limitations arise not

93   only because of the magnitude of the computational burden but also because of the convergence

94   properties of the numerical solution. To develop an operational-type radar algorithm for the DPR

95   snow retrieval, it is desirable to have a scattering model that provides efficient computation at an

96   arbitrary frequency over a large range of particle sizes. Comparisons of the scattering results

97   between simple and more complicated snow models indicate that the scattering properties of

98   aggregates at the DPR frequencies are fairly well reproduced by randomly-oriented ellipsoidal

99   particles if the effective mass density of snow is constant with size (Liao et al. 2013). By taking

100   advantage of both developed scattering databases and simple scattering models, we attempt to

101   employ the scattering results of the aggregates from the scattering database for small to moderate

102   particle sizes and use the results from the simple scattering models for large particles to cover the

103   full range of particle sizes for characterizing snow scattering properties at Ku- and Ka-band.

104

105   One of the DPR algorithms for snow retrieval employs a fixed-snow-density spherical model for

106   computations of the Ku- and Ka-band radar backscattering and extinction cross sections using

107   the assumption of an exponential PSD (Seto et al. 2013). To improve snow retrieval accuracy,

108   we will investigate retrieval uncertainties associated with the PSD and the particle scattering

109   models, and introduce new forms of the retrieval look-up tables that directly link DPR Ku- and

110   Ka-band radar reflectivities to snow water content and snowfall rate without the use of derived

111   PSD parameters. Newly formed look-up tables provide an effective means not only for snow

112   retrieval but for analysis of the retrieval uncertainties associated with the PSD model and the

113   particle scattering models. In order to check the consistency of the snow retrievals,

114   measurements of the snow PSD and fall velocity acquired from the Snow Video Imager/Particle

115   Image Probe (SVI/PIP) are used (Newman et al. 2009). It is believed that a collection of long-

116   term PSD data, fall velocities and information on particle mass spectra will provide a strong

117   basis for evaluating the performance of the DPR Ku- and Ka-band techniques.

118

119   This article is organized as follows. Methods for snow retrieval are described in Section 2, and

120   measurements of the PSD are discussed in Section 3, followed by remarks and a summary in

121   Section 4.

122
123   **2   Technical Approach and Methodology**
124

125   Understanding the retrieval errors associated with the snow particle size/mass distributions

126   models and particle scattering models employed by the DPR algorithms is important for the

127   evaluation of algorithm performance. The study also provides insight into which of the models

128   yield the most accurate DPR estimates of snow. Proper selection of the PSD and scattering

129   models can improve the overall performance of the DPR profiling algorithm. What follows are

130   discussions of snow scattering models and the parameterization of the particle size spectra and

131   how these models affect the radar retrievals.

132

133   2.1   Single scattering model of snow aggregates

134

135   Several simulated aggregate models have been developed using the pristine ice crystal habits

136   found in nature as the basic elements from which the aggregates are constructed (Draine and

137   Flatau 1994; Liu 2004 and 2008; Weinman and Kim 2007; Petty and Huang 2010; Botta et al.

138   2010 and 2011; Nowell et al. 2013; Kuo et al. 2016). For these particles, a numerical scheme is

139   required to compute the scattered fields. Although these numerical computations are useful, they

140   are time consuming, and are often limited to small-to-moderate particle sizes for a limited set of

141   frequencies. A few scattering databases derived from simulated aggregates are available (Nowell

142   et al. 2013; Kuo et al. 2016), but the maximum equivalent ice diameter is limited to around 2.5-3

143   mm which is not large enough to cover entire particle size range.

144

145   To account for the scattering contribution from the entire particle size range, the current DPR

146   algorithms adopt a simple scattering model, namely, the ice-air mixed spheres with a fixed snow

147   density of 0.1 g/cm^3 for all particle sizes (Seto et al. 2013). To check the validity and accuracy of

148   the simple geometric scattering model, a study was carried out by Liao et al. (2013) in which

149   scattering results from aggregates comprised of 6-branch bullet rosette crystals were compared

150   with those obtained from spherical or spheroidal ice-air mixed phase particles. Shown in Fig.1 is

151   an example of these results, in which backscattering (left) and extinction (right) coefficients at

152   35.6 GHz are plotted versus the equivalent ice diameter for 3 simulated snow aggregates and

153   results from the sphere, oblate and prolate spheroids. A constant effective snow density of 0.2

154   g/cm^3 is assumed for all spherical and spheroidal particle models. The spheroids are assumed to

155   be randomly oriented, i.e., their symmetry axes are uniformly distributed in three-dimensional

156   space. The aspect ratios (γ) of the spheroids, defined as the ratio of polar to equatorial lengths,

157   are taken to be either 0.5 or 2 to represent oblate and prolate spheroids respectively. The results

158   of the study show that the scattering properties of the aggregates are fairly well reproduced by an

159   equivalent-mass spheroidal particle when a constant snow density is assumed.

160

161   Agreement between the spheroidal/fixed density model and the aggregates suggests the validity

162   of the simple model and its utility for computing look-up tables for the DPR. An effective snow

163   density of 0.2 g/cm^3 is best able to reproduce the scattering parameters of the bullet-rosette

164   aggregates at the DPR frequencies. It is important to note that the effective mass density, as

165   defined in this paper, is that mass density of a spheroidal particle whose associated scattering

166   parameters provide the best match to those of the simulated aggregates with the same mass. This

167   definition is motivated by the desire to match the scattering properties of the spheroidal and

168   simulated aggregates and is distinct from the usual definition of snow density given by the ratio

169   of the particle mass to the volume where the volume is taken to be that of a circumscribing

170   sphere or spheroid. To distinguish our definition from others, the density we use for scattering

171   computations is referred to as the effective snow density. It is also important to note that the

172   snow mass is preserved in both definitions; that is, the product of the mass density or effective

173   mass density and the particle volume yields the same mass.

174

175   Recently, Kuo et al. (2016) have developed a comprehensive scattering database, which is

176   computed using the discrete dipole approximation (DDA) from a collection of realistic

177   aggregates simulated from a 3-D growth model with mass vs. size and fractal properties that are

178   consistent with field observations (Gravner and Griffeath 2009). Because of its limited range of

179   particle size mentioned earlier, the scattering tables of snow aggregates in our study will be taken

180   as a hybrid form that combines the scattering results from the Kuo et al. scattering database for

181   small to moderate particle sizes and the results from the simple scattering models for large

182   particles. Illustrated in Figs.2 and 3 are these scattering results at Ku- and Ka-bands from the

183   Kuo et al. database along with the results from an oblate spheroidal model for particle diameters

184   up to 6 mm. The results from the simple models (red curves) are those obtained from the

185   randomly-oriented oblate spheroids with an aspect ratio of 0.7 and a constant effective mass

186   density of 0.2 g/cm^3. The results of the scattering tables, which are denoted by the term "fitted"

187   and shown by the black curves, represent the mean values of the data from the scattering

188   database, where the mean is taken from all types of aggregates having the same mass, and the

189   results from the 0.2 g/cm^3 oblate spheroid model in the size range where the scattering database

190   is unavailable. The maximum liquid equivalent diameters of the current Kuo et al. database at

8

191   Ku- and Ka-bands are 3 and 2 mm, respectively. In other words, the scattering results from the

192   simple models are employed in the tables for the size ranges from 3-6 mm at Ku-band and 2-6

193   mm at Ka-band. The fairly good agreement of the scattering results in Figs. 2 and 3 between the

194   simple model and the scattering database (with mean differences less than 10% for the

195   backscattering and 7% for extinction cross sections) over the size range where the database is

196   valid suggests the validity of the simple models for the smaller particle sizes. As the scattering

197   database is updated to cover larger particle sizes, the validity of the simple scattering model will

198   be reassessed.

199

200   2.2   Particle size/mass distribution model

201

202   The three-parameter gamma distribution is one of the most common ways to mathematically

203   describe hydrometeor size/mass distributions (Gorgucci et al. 2000 and 2002; Bringi et al. 2002).

204   The form of the gamma distribution is expressed as

$$N(D) = N_W f(\mu)\left(\frac{D}{D_m}\right)^{\mu} \exp(-\Lambda D), \tag{1}$$

206   where D_m is the mass-weighted diameter of the particle, N_w is a scale factor, and μ is the shape

207   factor where

$$f(\mu) = \frac{6(4+\mu)^{\mu+4}}{4^4 \Gamma(\mu+4)} \quad \text{and} \quad \Lambda = (4+\mu)/D_m, \tag{2}$$

209   To describe snow particle size and mass spectra, the PSD in (1) and (2) is given as a function of

210   liquid equivalent or melted diameter D, which is also called particle melted-size distribution. D_m

211   is the melted median mass diameter, defined by

212

9

213
$$D_m = \frac{\int_0^\infty D^4 N(D) dD}{\int_0^\infty D^3 N(D) dD}.$$
(3)

214

215 In the inner swath, the DPR provides Ku- and Ka-band reflectivity factor measurements at each

216 range gate so only two parameters of the PSD can be determined. Typically, the shape factor (μ)

217 is taken to be constant. Although μ is often set to zero (exponential distribution) (Gunn and

218 Marshall 1958; Seto et al. 2013), the impact of this choice on the retrieval needs to be

219 investigated.

220

221 The differential frequency ratio (DFR), which is defined as the difference between the radar

222 reflectivity factors at Ku- and Ka-bands in decibels, is perhaps the most important quantity for

223 the dual-wavelength radar techniques in estimating hydrometeor micro/macro-physical

224 properties. As the DFR is independent of N_w, D_m can be derived from the DFR relations once μ

225 has been fixed. However, the DFR-D_m relation depends not only on μ but on the particle shape,

226 orientation distribution and mass density. Fig.4 provides the results of DFR as a function of the

227 liquid equivalent median mass diameter using a randomly-oriented, fixed density spheroidal

228 particle model. The left plot shows the variations in the DFR-D_m relation resulting from

229 different effective snow densities. Computations of the radar scattering parameters at different

230 effective snow densities are made in the same way as in the case of 0.2 g/cm^3. The particle sizes

231 (semi axes of spheroid) are solely determined by the density specified for a given particle mass.

232 The center plot shows the effects of particle shape where a γ value of 1 corresponds to a sphere

233 while γ values less than 1 correspond to an oblate spheroid. The plot on the right shows the

234 effect of changing μ. Analysis of these results indicates that particle shape has a small effect on

235   the DFR-D_m relation and changes the results by less than 4% for changes in γ from 0.5 to 1 while

236   the shape factor leads to the change in the results of no more than 20%. On the other hand, the

237   DFR-D_m relation has a strong dependence on the effective snow density. In other words, the

238   determination of D_m from the DFR is relatively insensitive to μ and to particle shape, if the

239   orientation is random, whereas the relationship is quite sensitive to the effective snow density

240   used for computations of the scattering parameters. As can be seen in Figs.1-3, the extinction

241   coefficients at both Ku- and Ka-bands, though in good agreement between the simple model and

242   the scattering database, are small and can usually be neglected. It should be noted that the above

243   conclusions are based on the assumption of random orientation of the aggregates. When this

244   assumption is violated, then the orientation distribution as well as particle shape become

245   important.

246

247   Although an effective snow density of 0.2 g/cm^3 is found to be suitable for the computations of

248   the Ku- and Ka-band radar scattering parameters for equivalent ice diameters up to 2-3 mm,

249   further testing will be necessary to assess this assumption when scattering results from larger

250   aggregates become available. It is worth noting that the results of Liao et al. (2013) show

251   reasonably good agreement between radar scattering parameters at higher frequencies (from 89-

252   183.31 GHz) as derived from the simple models and the simulated aggregates for particle

253   diameters up to 2.5 mm despite the fact that the simple models using spheres or nearly spherical

254   particles produce backscattering results with more pronounced oscillations (resonance effects)

255   than the aggregate results. This is encouraging in the sense that it shows that an effective density

256   of 0.2 g/cm^3 yields good agreement with the simulated aggregate results for electrically larger

257   particles. On the other hand, it might be the case that the effective snow density may need to be

258 changed for larger particle types so as to ensure good agreement. In either case, the objective is

259 to provide scattering tables at all relevant frequencies and particle sizes that incorporate the most

260 recent scattering results.

261

262 2.3   Dual-wavelength retrieval algorithm

263

264 As discussed above, D_m can be derived from the DFR-D_m relations for a given μ. In principle,

265 once D_m is determined, N_w is derived using the radar reflectivity at either Ku- or Ka-band.

266 Subsequently, snow water content (SWC) and equivalent snowfall rate (R_S) can be computed

267 from the derived PSD parameters. The fall velocity of snow is needed in order to estimate R_S.

268 For the development of an effective dual-wavelength radar retrieval technique, it is desirable to

269 employ look-up tables (LUT) that are formed in such a way that the radar measurements are

270 directly linked to the microphysical properties of snow (D_m and N_w) and its associated bulk

271 parameters (SWC and R_S). With use of the LUTs different particle models and their scattering

272 properties can be evaluated separately in the context of the same algorithm.

273

274 Illustrated in Fig.5 are such tables in which SWC (top-left), R_S (top-right), D_m (bottom-left) and

275 N_w (bottom-right) along the ordinate are given as a function of the DFR. A flowchart is provided

276 in Fig.6 showing the procedures to compute the radar reflectivitity factors and snow size and

277 bulk hydrometeor parameters from an assumed mass spectrum model. In Fig.5, SWC, R_S, N_w

278 have been normalized by the Ku-band radar reflectivity factor so that they can be expressed

279 solely as a function of DFR for given PSD and scattering models. The way to normalize liquid

280 water content by reflectitities has previously been adopted in the study of ice clouds (Hogan et

12

281   al. 2000; Botta et al. 2013). The results in Fig.5 are computed under the assumption that the

282   snow particles are fixed-density, randomly-oriented oblate spheroids with an aspect ratio of 0.7

283   that follow an exponential particle size distribution. As an example, and also for reference, the

284   tables are plotted in Fig.5 for effective snow densities varying from 0.05 to 0.5 g/cm^3. The

285   terminal velocities of snowflakes used for the computations of R_S are based on the results of

286   Magono and Nakamura (1965). It is important to note that the results from the LUTs shown in

287   Fig.5 can be used to determine SWC and R_S as they directly link the DPR radar reflectivities to

288   SWC and R_S without use of the derived PSD parameters.

289

290   The procedure for the estimation of snow parameters is described as follows: given a pair of

291   reflectivity factors (Z_{Ku}, Z_{Ka}), the DFR in dB is defined as $10Log_{10}(Z_{Ku}/Z_{Ka})$, from which we find

292   the values of SWC/Z_{Ku} (left) and R_S/Z_{Ku} (right) for an assumed effective snow density. By

293   multiplying by Z_{Ku}, the results of SWC and R_S are then obtained. Obviously the values of SWC

294   and R_S depend on the effective snow density. The estimates of D_m and N_w can be achieved in a

295   similar way. It is worth mentioning again that snow attenuations, though correctable, are

296   typically negligibly small for most Ku- and Ka-band spaceborne radar measurements.

297

298   As LUTs change with different scattering models and PSD parameterizations, a proper selection

299   of the tables is critical to the accuracy of the retrieval. It is instructive to conduct a sensitivity

300   study with respect to the model assumptions and to gain an understanding of the uncertainties

301   associated with each of the models. Figure 7 provides such a sensitivity study in which the LUTs

302   are checked against 3 μ values. Similar to the findings in Fig.4, a change in μ leads to changes in

303   the estimates of SWC and R_S of less than 20% so that the assumption of μ equal to zero, as found

13

304   in many observations, yields a reasonable approximation for the estimates of snow. Although it

305   is worth testing the scattering databases of the aggregates formed from various crystal habits, it is

306   not the focus of the study to evaluate and validate these scattering databases. Because the mass

307   of the aggregates is the dominant factor in the scattering parameters at Ku- and Ka-bands,

308   significant differences among the various scattering databases are not expected. This is

309   evidenced by the fact of that there is good agreement between the scattering databases derived by

310   Nowell et al. (2013) and Kuo et al. (2016) and that the small variations of the scattering and

311   extinction coefficients as computed from various aggregate models (Kuo et al. 2016) can be seen

312   from the variations in the data (blue) shown in Figs.2-3.

313

314   **3   Assessment of snow retrieval: PSD model assumptions**

315

316   Because of the complexity of snowfall processes and the difficulties encountered in accurately

317   measuring the microphysical properties, validating snow estimates is a challenging task. With the

318   advent of more advanced digital cameras and image processing technologies, measurements of

319   falling snow have been improved to the point where the snow particle size spectra and fall

320   velocities can be obtained fairly accurately (Bohm 1989; Huang et al. 2010 and 2015; Garrett et

321   al. 2012). An independent and direct measurement of the mass of individual snow particles is,

322   however, still a difficult task, and therefore direct measurements of the snow mass spectrum are

323   rarely available. Several investigations into deriving snow mass spectra are being pursued, which

324   are in fact part of the effort in the GPM ground validation project. These methods are based on

325   the principle that particle masses can be related to their fall velocities after accounting for air

326   drag and other aerodynamics effects (Bohm 1989; Heymsfield et al. 2010). Understanding the

327   microphysical properties of snow should further improve our ability to generate better scattering

14

328 representations and more accurate look-up tables for retrieving snow bulk properties from the

329 DPR. It would be ideal to evaluate snow retrievals with co-located dual-wavelength radar

330 measurements and in situ snow microphysical measurements. These data, though desirable, are

331 not available. Our attention is therefore focused on the assessment of the PSD assumptions used

332 in developing the retrieval algorithms using measured PSD.

333 To check the consistency of snow retrievals using the LUTs, measurements of snow spectra are

334 used. The data were obtained from 8 snow events during winter of 2014 taken at the NASA

335 Wallops Flight Facility in Wallops Island, Virginia using the Snow Video Imager/Particle Image

336 Probe (SVI/PIP). Table 1 provides details of these events that include starting and ending times

337 of snowfall, mean temperature as well as total accumulations of each event. In Wallops Island

338 annual mean snowfall is about 200.66 mm, and in 2014 it was recorded to be 223.66 mm,

339 slightly more than average. Although the PIP measures the dimensions or sizes of the

340 snowflakes and their fall velocities, it does not provide measurements of particle mass. In order

341 to compute the radar reflectivities and snow bulk parameters as in (4) and (5), the mass spectra or

342 melted size spectra are needed. Conversion of the PSD measurements to the mass spectra,

343 however, relies on the empirical mass-size relations. There are many such relationships available

344 in the literature that can be used to derive m(D) (Nakaya 1954; Magono and Nakamura 1965;

345 Zikmunda and Vali 1972; Locatelli and Hobbs 1974; Mitchell et al. 1990; Brandes et al. 2007;

346 Heymsfield et al. 2010). These results show some variability depending on snow type, amount of

347 riming and other conditions under which the measurements were made. In this study, two well-

348 known mass-size relations, the results from Heymsfield et al. (2010) and Brandes et al. (2007),

349 are used to test how the estimates of snow change with use of different mass-size relations when

350 the same LUTs are used.

351

352 An example of the PSD measurements is shown in Fig.8, in which N(D) of the PSD (top), shown

353 along the vertical with the amplitude of the spectrum given by the color scale, is given as a

354 function of time. The equivalent snowfall rate (middle) and median mass diameter (D_m) (bottom)

355 are also shown for the same time period. For the computations of snowfall rate and D_m, empirical

356 snow mass-size relations are used in conjunction with the measured snow particle size spectra

357 and fall velocities. The following equations are used for obtaining R_S and D_m:

$$D_{m=}\frac{\int_0^\infty D\, m(D)N(D)dD}{\int_0^\infty m(D)N(D)dD}, \qquad (4)$$

$$R_S = \frac{36\times10^{-4}}{\rho_w}\int_{D_{min}}^{D_{max}} N(D)\, m(D)V(D)dD, \qquad (5)$$

360 where D and D_m in (4) and (5) as well as in Fig.8 are, respectively, the actual particle diameter

361 and median mass diameter rather than the melted sizes employed in the rest of the paper. m(D)

362 is the particle mass-size relation, and ρ_w is the water mass density taken to be 1 g/cm^3. Note also

363 that the data shown in Fig. 8 represent a measurement period of 1000 minutes of snow data

364 (~three snow events) with a one-minute integration time. The mass-size relation of Heymsfield et

365 al. (2010) is used for computations of R_S and D_m.

366

367 Illustrated in Fig.9 are the scatter plots (red dots) of SWC (top row) and R_S (bottom row)

368 computed from the measured PSD with use of mass-size relations when the hybrid scattering

369 tables are assumed. For reference, the LUTs derived from the constant effective density

370 scattering models as shown in Fig.6 are superimposed in Fig.9. The SWC and R_S as well as the

371 quantities associated with the Ku- and Ka-band radar reflectivities shown in Fig.9 are obtained

372 from a total of about 8000 1-minute PSD measurements collected from the PIP during the winter

373   of 2014 at Wallops using the mass-size relations of Brandes et al. (left column) and Heymsfield

374   et al. (right column). Mass-size relations are used to convert the measured particle size

375   distribution (PSD) to the melted size distribution from which the scatterings and snow bulk

376   parameters can be computed as in (2)-(5). The mass-size relations used in Fig.9 are those from

377   Eq.(8) of Brandes et al. (2007) and Eq.(10) of Heymsfield et al. (2010). The procedures used in

378   obtaining the radar parameters and SWC and R_S from the measured PSD are shown in the flow

379   diagram of Fig.10. Analysis of the SWC results indicates that the snow water content derived

380   from the measured PSD agree reasonably well with those from the tables when the effective

381   snow density is taken to be 0.2 g/cm^3. Because the scattering table, which is a hybrid formed

382   from the mean aggregate solution at small particle sizes with the spheroidal particle model at

383   larger sizes, used for computing the reflectivities of the measured PSD and the scattering results

384   with a density of 0.2 g/cm^3 are nearly the same as shown in Figs.2-3, the differences in snow

385   water content between the measured PSD and the table results from a density of 0.2 g/cm^3 are

386   mostly caused by the differences between measured and modeled melted particle size

387   distributions. As noted earlier, the exponential melted-size distribution is assumed in the look-up

388   tables while the measured melted-size distribution is derived from the measured particle diameter

389   spectrum and the mass-size relation that generally will be different from an exponential

390   distribution. Computation of the snowfall rate, on the other hand, depends not only on the

391   particle mass (or melted-size) spectrum but also on the particle fall velocities. Most of the

392   estimated snowfall rates, as derived from the measured PSD and the mass-size relations, and

393   shown in the lower panels of Fig.9, lie between the table results with effective densities of 0.1

394   and 0.2 g/cm^3. The mean differences of the SWC between the 0.2 g/cm^3 snow density LUTs and

395   the PSD-derived results are about 20% for Ku-band radar reflectivities greater than 15 dBZ (the

396   approximate minimum detectable signal of the DPR Ku-band channel). Larger differences

397   between the R_S estimates are found, and can be attributed to differences in the snow fall velocity

398   spectra between the measured and modeled mass distribution. The terminal velocities of

399   snowflakes used for the computations of the LUTs are based on the results of Magono and

400   Nakamura (1965) while the measured fall velocities are used for the computations of PSD

401   snowfall rate.

402

403   The overall agreement of the snow water content between the results from the measured PSD

404   and the results from the LUTs suggests that the exponential particle distribution model assumed

405   in the tables is reasonable. Different mass-size relations lead to different mass spectra for a given

406   measured PSD. That the retrieval results from the Brandes et al. and Heymsfield et al. mass-size

407   relations follow the trends of SWC and R_S similar to those derived from the LUTs further

408   suggest that the Ku- and Ka-band dual-wavelength techniques adopted are relatively insensitive

409   to the choice of either the Brandes or the Heymsfield mass-size relation. These results

410   approximately yield the table values obtained from the 0.2 g/cm^3 snow density. It is also worth

411   mentioning that the results from the measured PSD are relatively insensitive to PSD integration time even

412   though the scatter in the data is slightly reduced if a longer integration is used.

413

414   **4   Summary**

415

416   The ultimate goal of this study is to better understand the estimation process in retrieving snow

417   microphysical properties (N_w and D_m) and the associated bulk parameters (SWC and R_S) for

418   improvement of the Ku- and Ka-band dual frequency radar retrieval. This is done by first finding

419   suitable single scattering tables and PSD models and then using this information to construct

420   snow retrieval look-up tables. Presently available scattering databases, though accurate and

421   useful, are limited to small and moderate particle sizes. To extend the results to larger sizes, a

422   simple scattering model that agrees well with the scattering databases at small particle sizes is

423   used. It is found that a snow particle model consisting of randomly oriented oblate spheroids

424   with an effective mass density of 0.2 g/cm^3 yields good agreement with the results from the

425   scattering databases at Ku- and Ka-band. Thus the single-particle scattering database is a hybrid

426   that uses the scattering database for small and moderate particles and a simple randomly oriented

427   oblate with a constant effective mass density of 0.2 g/cm^3 for large particles.

428

429   Using single scattering tables and an assumed PSD model, the Ku- and Ka-band radar

430   reflectivity factors and snow bulk parameters are computed. Thus, the relationships between the

431   results of DFR and SWC and R$_S$ are established to form the dual-wavelength radar retrieval look-

432   up tables. Retrievals of snow water content and snowfall rate, as the primary focus of this study,

433   are therefore achieved by using newly introduced look-up tables that directly link Ku- and Ka-

434   band radar reflectivities to hydrometeor parameters without the use of derived PSD parameters.

435   The look-up tables are formed so that SWC and R$_S$, both of which are normalized by the Ku-

436   band radar reflectivity factor, are expressed as a function of the differential frequency ratio of

437   Ku- and Ka-bands. The look-up tables offer not only computational advantages but provide

438   direct insight into how the model assumptions impact the retrieval results. The nature of one-to-

439   one relations between the normalized hydrometeor parameters and DFR provides a means to

440   obtain unique solutions of the snow parameters for a given PSD and single scattering model. To

441   understand the uncertainties in the snow estimates associated with the PSD parameterizations

442   and scattering models, a sensitivity study was done, finding that the choice of shape factor of the

443   gamma PSD has only a slight impact on the retrievals. As such, a value of μ of zero, as

444   supported by some observations, should yield reasonable estimates of snow parameters from the

445   perspective of dual-wavelength radar retrieval.

446

447   Self-consistency of the snow retrievals has been checked using measurements of snow PSD and

448   fall velocity acquired from the PIP during the winter of 2014 in Wallops. Among several

449   assumptions that have been examined are conversions to particle mass spectra using different

450   mass-size relations, scattering particle models and snow PSD. Analysis of nearly 8000 1-minute

451   PSD measurements suggests that exponential PSD model ($\mu=0$) is sufficiently accurate for the

452   dual-wavelength radar retrieval of snow bulk parameters. It also indicates that the use of either

453   the Heymsfield or the Brandes mass-size relation yields approximately the same snow estimates.

454   However, these findings should be viewed as preliminary because of the limited data

455   measurements at a single location. Collections of long-term PSD data, fall velocities and

456   information on particle mass spectra at multiple sites will provide further evaluation of the

457   performance of the Ku- and Ka-band radar techniques. Further tests of the scattering tables will

458   be done by comparing the accuracy of the simple particle model against scattering results from

459   larger simulated aggregates, as these results become available.

460

466

467   Appendix

468   List of Symbols and Acronyms

469   GPM: Global Precipitation Measurement
470   DPR: Dual-frequency Precipitation Radar
471   NASA: National Aeronautics and Space Administration
472   JAXA: Japan Aerospace Exploration Agency
473   Ku-band: Frequency of 13.6 GHz
474   Ka-band: Frequency of 35.6 GHz
475   PSD: Particle Size Distribution
476   SVI/PIP: Snow Video Imager/Particle Image Probe
477   DDA: Discrete Dipole Approximation
478   N(D):   Particle Size Distribution
479   N_W: Scale Factor of Particle Size Distribution
480   μ: Shape Factor of Gamma Distribution
481   D: Particle Diameter
482   D_m: Mass-weighted Diameter
483   Λ: Slope Parameter
484   DFR: Differential Frequency Ratio
485   SWC: Snow Water Content
486   R_S: Equivalent Snowfall Rate
487   LUT: Look-up Table
488   Z_{Ku}:   Ku-band Radar Reflectivity Factor
489   Z_{Ka}:   Ka-band Radar Reflectivity Factor
490   m(D):   Particle Mass as Function of Particle Diameter
491   V(D):   Particle Fall Velocity
492   ρ_w: Liquid Mass Density
493   ρ_s: Snow Mass Density
494   D_{min}:   Minimum Diameter
495   D_{max}:   Maximum Diameter
496   f: Frequency
497   γ: Aspect Ratio of Particle
498

499

References

500

501   Brandes, E., K. Ikeda, G. Zhang, M. Schoenhuber, and R. Rasmussen, 2007: A statistical and
502   physical description of hydrometeor distributions in Colorado snowstorms using a video
503   distrometer. *J. Appl. Meteor. Climat.*, **46**, 634-650.
504

505   Bohm, H.P., 1989: A general equation for the terminal fall speed of solid hydrometeors. *J.*
506   *Atmos. Sci.*, **46**, pp. 2419-2427.
507

508   Botta, G., K. Aydin, and J. Verlinde, 2010: Modeling of microwave scattering from cloud ice
509   crystal aggregates and melting aggregates: A new approach. *IEEE Geo. Rem. Sens. Lett.*, **7**,
510   572-576.
511

512   Botta, G., K. Aydin, J. Verlinde, A.E. Avramov, A.S. Ackerman, A.M. Fridlind, G.M.
513   McFarquhar and M. Wolde, 2011: Millimeter wave scattering from ice crystal aggregates:
514   Comparing cloud model simulations with X- and Ka-band radar measurements. *J. Geophys.*
515   *Res.*, **116**, D00T04.
516

517   Botta, G., K. Aydin, and J. Verlinde, 2013: Variability in millimeter wave scattering properties
518   of dendritic ice crystals. *J. Quant. Spectrosc. Radiat. Transf.*, **131**, 105-104.
519

520   Bringi, V., G. Huang, V. Chandrasekar and E. Gorgucci, 2002: A methodology for estimating the
521   parameters of a Gamma raindrop size distribution model from polarimetric radar data:
522   Application to a squall-line event from the TRMM/Brazil campaign. *J. Oceanic and Atmos.*
523   *Tech.,* **19**, 633-645.
524

525   Draine, B. T., and P. J. Flatau, 1994: Discrete dipole approximation for scattering calculations. *J.*
526   *Opt. Soc. Am. A.*, **11**, 1491-1499.
527

528   Garrett, T. J., Fallgatter, C., Shkurko, K., and Howlett, D., 2012: Fall speed measurement and
529   high-resolution multi-angle photography of hydrometeors in free fall. *Atmos. Meas. Tech.,* **5**,
530   2625-2633.
531

532   Gorgucci, G. Scarchilli, V. Chandrasekar and V. Bringi, 2000: Measurement of mean raindrop
533   shape from polarimetric radar observations. *J. Atmos. Sci.*, **57**, 3406-3413.
534

535   Gorgucci, E., G. Scarchilli, V. Chandrasekar, and V. Bringi, 2002: Estimation of raindrop size
536   distribution parameters from polarimetric radar measurements. *J. Atmos. Sci.,* **59**, 2373-
537   2384.
538

539   Gravner, J., and D. Griffeath, 2009: Modeling of snow-crystal growth: A three dimensional
540   mesoscopic approach. *Phys. Rev. E*, **79**, 011601.
541

542   Gunn, K. L. S., and J.S. Marshall, 1958: The distribution with size of aggregate snowflakes. *J.*
543   *Meteor.*, **15**, 452-461.
544

Heymsfield, A. J., Z. Wang, and S. Matrosov, 2005: Improved radar ice water content retrieval algorithms using coincident microphysical and radar measurements. *J. Appl. Meteor.*, **44**, 1391–1412.

Heymsfield, A. J., and C. D. Westbrook, 2010: Advances in the estimation of ice particle fall speeds using laboratory and field measurements. *J. Atmos. Sci.,* **67**, 2469–2482.

Heymsfield, A. J., C. Schmitt, A. Bansemer, and C. H. Twohy, 2010: Improved representation of ice particle masses based on observations in natural clouds. *J. Atmos. Sci.*, **67**, 3303–3318.

Hogan, R., A. Illingworth, and H. Sauvageot, 2000: Measuring crystal size in cirrus using 35- and 94-GHz radars. *J. Atmos. Oceanic Technol.*, **17**, 27-37.

Hou, A., G. S. Jackson, C. Kummerow, and C. M. Shepherd, 2008: Global precipitation measurement. Precipitation: Advances in Measurement, Estimation, and Prediction, S. Michaelides, Ed., Springer, 131–169.

Hou, A. Y., R. K. Kakar, S. Neeck, A. A. Azarbarzin, C. D. Kummerow, M. Kojima, R. Oki, K. Nakamura, and T. Iguchi, 2014: The global precipitation measurement mission. *Bull. American Meteor. Soc.*, **95**, 701-722.

Huang, G., Bringi, V. N., Cifelli, R., Hudak, D. and Petersen, W. A., 2010: A Methodology to Derive Radar Reflectivity‐Liquid Equivalent Snow Rate Relations Using C-Band Radar and a 2D Video Disdrometer. *J. Atmos. Oceanic Technol.*, **27**, 637-651.

Huang, G., V.N. Bringi, D. Moisseev, W.A. Petersen, L. Bliven and D. Hudak, 2015: Use of 2D-video disdrometer to derive mean density–size and Ze–SR relations: Four snow cases from the light precipitation validation experiment, *Atmos. Res.*, **153**, 34–48.

Kuo, K-S, W. S. Olson, B. T. Johnson, M. Grecu, L. Tian, T. L. Clune, B. H. van Aartsen, A. J. Heymsfield, L. Liao, and R. Meneghini, 2016: The microwave radiative properties of falling snow derived from realistic ice particle models. Part I: An extensive database of simulated pristine crystals and aggregate particles, and their scattering properties. *J. Appl. Meteorol. Climatol.*,.55, 691-708.

Liao, L., R. Meneghini, H. Nowell and G. Liu, 2013:Scattering computations of snow aggregates from simple geometrical particle models. *IEEE J. Selected Topics in Earth Obs. and Remote Sens.*, **6**, 1409-1417.

Liu, G., 2004: Approximation of single scattering properties of ice and snow particles for high microwave frequencies. *J. Atmos. Sci.*, **61**, 2441-2456.

Liu, G., 2008: A database of microwave single-scattering properties for non spherical ice particles. *Bull. Am. Meteorol. Soc.*, **89**, 1563-1570.

590   Locatelli, J., and P. Hobbs, 1974: Fall speeds and masses of solid precipitation particles. *J.*
591   *Geophys. Res.*, **79**, 2185-2197.
592
593   Magono C., and T. Nakamura, 1965: Aerodynamic studies of falling snowflakes, *J. Meteorol.*
594   *Soc. Jpn.*, 43, 139–147.
595
596   Matrosov, S. Y., 1998: A dual-wavelength radar method to measure snowfall rate. *J. Appl.*
597   *Meteor.*, **37**, 1510–1521.
598
599   Matrosov, S. Y., A. J. Heymsfield, and Z. Wang, 2005: Dual-frequency ratio of non-spherical
600   atmospheric hydrometeors. *Geophys. Res. Lett.*, **32**, L13816, doi:10.1029/2005GL023210.
601
602   Mitchell, D. L., R. Zhang, and R. L. Pitter, 1990: Mass-dimensional relations for ice particles
603   and the influence of riming on snowfall rates. *J. Appl. Meteor.*, **29**, 153-163.
604
605   Nakaya, U., 1954: *Snow Crystals: Natural and Artificial*. Harvard University Press, 510pp.
606
607   Newman, A., P. A. Kucera, and L. Bliven, 2009: Presenting the snow video imager. *J. Atmos.*
608   *Ocean*. Technol., **26**, 167-179.
609
610   Nowell, H., G. Liu, and R. Honeyager, 2013: Modeling the microwave single-scattering
611   properties of aggregate snowflakes. *J. Geophys. Res. Atmos*., **118**, 7873–7885.
612   doi:10.1002/jgrd.50620.
613
614   Petty, G. W., and W. Huang, 2010: Microwave backscattering and extinction by soft ice spheres
615   and complex snow aggregates. *J. Atmos. Sci*., **67**, pp. 769-787.
616
617   Seto, S, T. Iguchi, and T. Oki, 2013: The basic performance of a precipitation retrieval algorithm
618   for the global precipitation measurement mission's single/dual-frequency radar
619   measurements. *IEEE Trans. Geosci. Remote Sens.*, **51**, 5239–5251.
620
621   Szyrmer, W., and I. Zawadzki, 2014a: Snow studies. Part III: Theoretical derivations for the
622   ensemble retrieval of snow microphysics from dual-wavelength vertically pointing radars. *J.*
623   *Atmos. Sci.,***71,** 1158–1170.
624
625   Szyrmer, W., and I. Zawadzki, 2014b: Snow studies. Part IV: Ensemble retrieval of snow
626   microphysics from dual-wavelength vertically pointing radars. *J. Atmos. Sci.,***71,** 1172–1186.
627
628   Wang, Z., G. M. Heymsfield, L. Li, and A. J. Heymsfield, 2005: Retrieving optically thick ice
629   cloud microphysical properties by using airborne dual-wavelength radar measurements. *J.*
630   *Geophys. Res.*, **110**, D19201, doi:10.1029/2005JD005969.
631
632   Weinman, J., and M.-J. Kim, 2007: A simple model of the millimeter-wave scattering parameters
633   of randomly oriented aggregates of finite cylindrical ice hydrometeors. *J. Atmos. Sci.*, **64**,
634   634-644.
635

636   Zikmunda, J., and G. Vali, 1972: Fall patterns and fall velocities of rimed ice crystals. *J. Atmos.*
637   *Sci.*, **29**, 1334-1347.
638

639   Table 1 Snow events during winter of 2014 in Wallops Island, Virginia

640

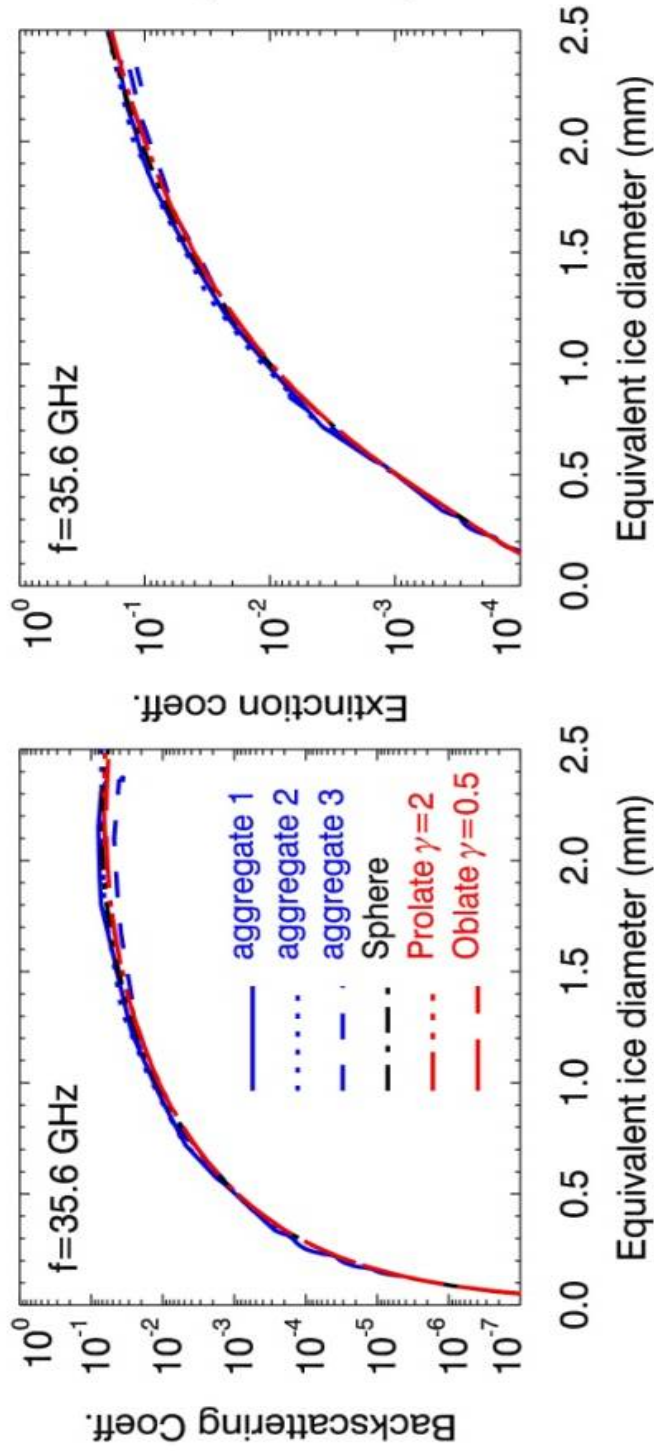| Events	Start Time (UTC)	End Time (UTC)	Accumulation (mm)	Mean Temperature (^{0}C)
1	JAN0305:09	JAN03 11:30	46.41	-1.4
2	JAN21 22:05	JAN22 10:03	5.52	-5.4
3	JAN28 20:41	JAN29 12:40	62.12	-9.5
4	FEB14 01:58	FEB14 05:12	6.37	1.9
5	FEB15 20:41	FEB15 23:23	0.76	2.2
6	MAR03 14:40	MAR03 22:00	34.15	-4.4
7	MAR17 08:04	MAR17 20:53	20.93	0.8
8	MAR25 18:50	MAR26 06:13	47.40	1.0

641

642   Figure captions:

643   Fig.1 Comparisons of backscattering (left) and extinction (right) coefficients of 3 snow
644   aggregates with the results from the sphere, oblate and prolate spheroids at a frequency of 35.6
645   GHz in terms of equivalent ice diameter. A constant snow density of 0.2 g/cm^3 is assumed for all
646   spherical and spheroidal particle models. The oblate and prolate spheroids are randomly oriented
647   with aspect ratios (γ) of 0.5 and 2, respectively.

648   Fig.2 Backscattering (left) and extinction (right) coefficients from the scattering database (blue
649   dots), simple scattering model (red curves), which is the randomly-oriented oblate spheroid with
650   a constant effective density of 0.2 g/cm^3 and an aspect ratio of 0.7, and scattering-database-
651   simple-model-combined results (black curves), also referred to as "fitted", at Ku band. The mean
652   values of the scattering results are used for the combined results over the data range.

653   Fig.3 Backscattering (left) and extinction (right) coefficients from the scattering database (blue
654   dots), simple scattering model (red curves), which is the randomly-oriented oblate spheroid with
655   a constant effective density of 0.2 g/cm^3 and an aspect ratio of 0.7, and scattering-database-
656   simple-model-combined results (black curves), also referred to as "fitted", at Ka band. The mean
657   values of the scattering results are used for the combined results over the data range.

658   Fig.4 The differential frequency ratio (DFR=10LOG$_{10}$(Z$_{Ku}$/Z$_{Ka}$)) as a function of equivalent-
659   liquid median mass diameter D$_m$. (Left): DFR-D$_m$ relations are plotted with several effective
660   snow densities (ρ_s) from 0.1 to 0.4 g/cm^3 as the shape factor (μ) of the gamma PSD is set to zero
661   and the aspect ratio (γ) of the oblate spheroid particles is set to 0.7. (Middle): DFR-D$_m$ relations
662   are plotted with the aspect ratios of 0.5, 0.7 and 1 at ρ_s=0.2 g/cm^3 and μ=0. (Right): DFR-D$_m$
663   relations are plotted with the values of μ of 0, 3 and 6 at ρ_s=0.2 g/cm^3 and γ=0.7.

664   Fig.5 The retrieval look-up tables that show the snow water content (SWC) (top-left) and
665   equivalent snowfall rate (R$_S$) (top-right), both of which are normalized by the Ku-band radar
666   reflectivity factor (Z$_{Ku}$), as a function of the DFR, defined by 10LOG$_{10}$(Z$_{Ku}$/Z$_{Ka}$), for several
667   effective snow densities (ρ_s) with the values from 0.05 to 0.5 g/cm^3. The liquid equivalent
668   median mass diameter D$_m$ (bottom-left) and the PSD scale parameter N$_w$ normalized by Z$_{Ku}$
669   (bottom-right) are also plotted in terms of DFR.

670   Fig.6 Flowchart of computing radar parameters and snow size and bulk properties.

671   Fig.7 The look-up tables used for the retrieval of SWC (left) and R$_S$ (right) with μ of 0, 3 and 6,
672   respectively, as computed from the single scattering tables depicted in Figs.2-3.

673   Fig.8 Example of a segment of the PSD measurements (1000 minutes) in time series taken from
674   8 snow events during winter of 2014 at the NASA Wallops Flight Facility using the SVI/PIP.
675   The particle size spectra (mm^{-1} m^{-3}), shown in the color scale, are given in the top panel while
676   equivalent snow fall rate and actual median mass diameter are displayed in the middle and

677   bottom panels, respectively. The PSD data, obtained by averaging the measurements over 1-

678   minute integration time, are merged from all the snow events into one data file with consecutive

679   time.

680   Fig.9 The snow water content (SWC) (top row) and equivalent snowfall rate (R_S) (bottom row),

681   both of which are normalized by the Ku-band radar reflectivity factor (Z_{Ku}), as a function of the

682   DFR, defined by $10LOG_{10}(Z_{Ku}/Z_{Ka})$, for several effective snow densities (ρ_s) with the values

683   from 0.05 to 0.5 g/cm^3. The scatter plots (red dots) are the results derived from the measured

684   PSD that were collected by the SVP/PIP from 8 snow events in the winter of 2014 at the NASA

685   Wallops Flight Facility. Two empirical density-size relationships reported by Brandes et al.

686   (2007) and Heymsfield et al. (2010) are used in converting the measured PSD to the snow mass

687   spectra, and the results from their respective relations are shown in the left and right panels.

688   Fig.10 Flowchart detailing the procedures of obtaining radar reflectivities and snow parameters.

689

690

691

692

693

694

695

696

697

698

699

700

701

Fig.1 Comparisons of backscattering (left) and extinction (right) coefficients of 3 snow aggregates with the results from the sphere, oblate and prolate spheroids at a frequency of 35.6 GHz in terms of equivalent ice diameter. A constant snow density of 0.2 g/cm^3 is assumed for all spherical and spheroidal particle models. The oblate and prolate spheroids are randomly oriented with aspect ratios (γ) of 0.5 and 2, respectively.
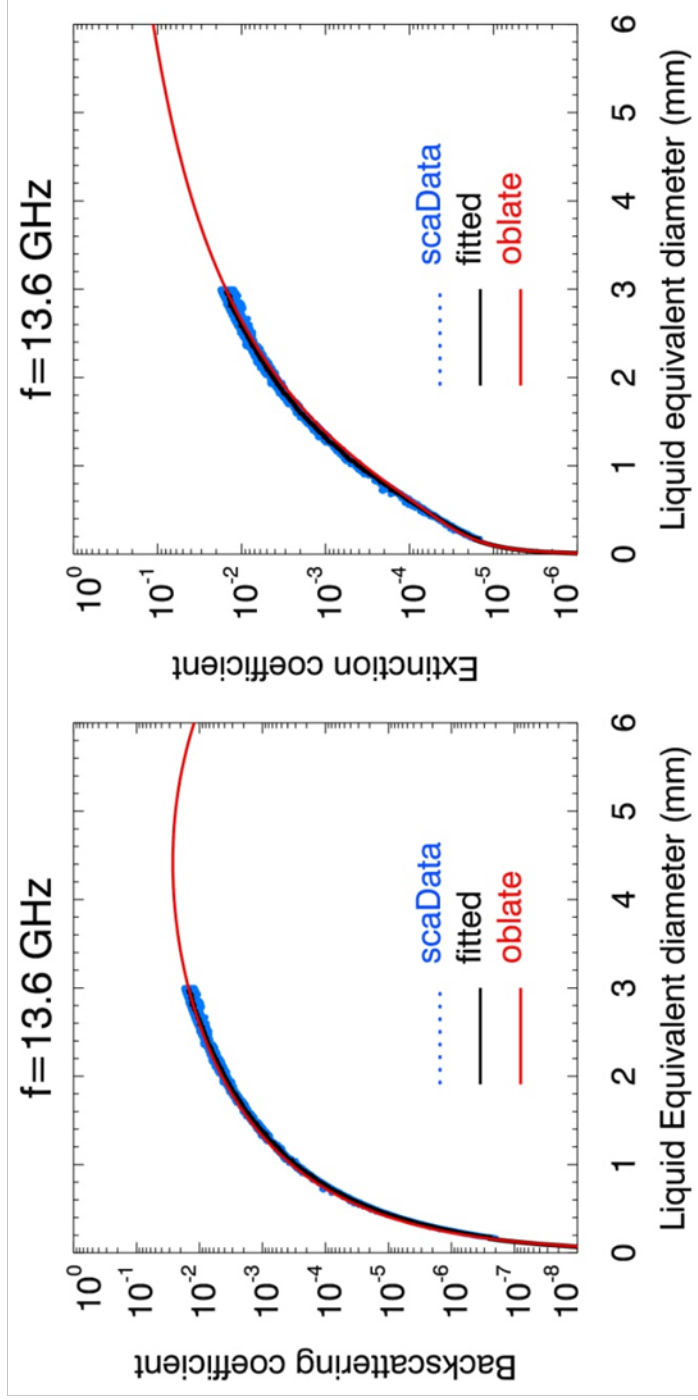
702

703

704

Fig.2 Backscattering (left) and extinction (right) coefficients at Ku-band from the scattering database (blue dots), simple scattering model (red curves), which is the randomly-oriented oblate spheroid with a constant effective density of 0.2 g/cm³ and an aspect ratio of 0.7, and scattering-database-simple-model-combined results (black curves), also referred to as "fitted". The mean values of the scattering results are used for the combined results over the data range.
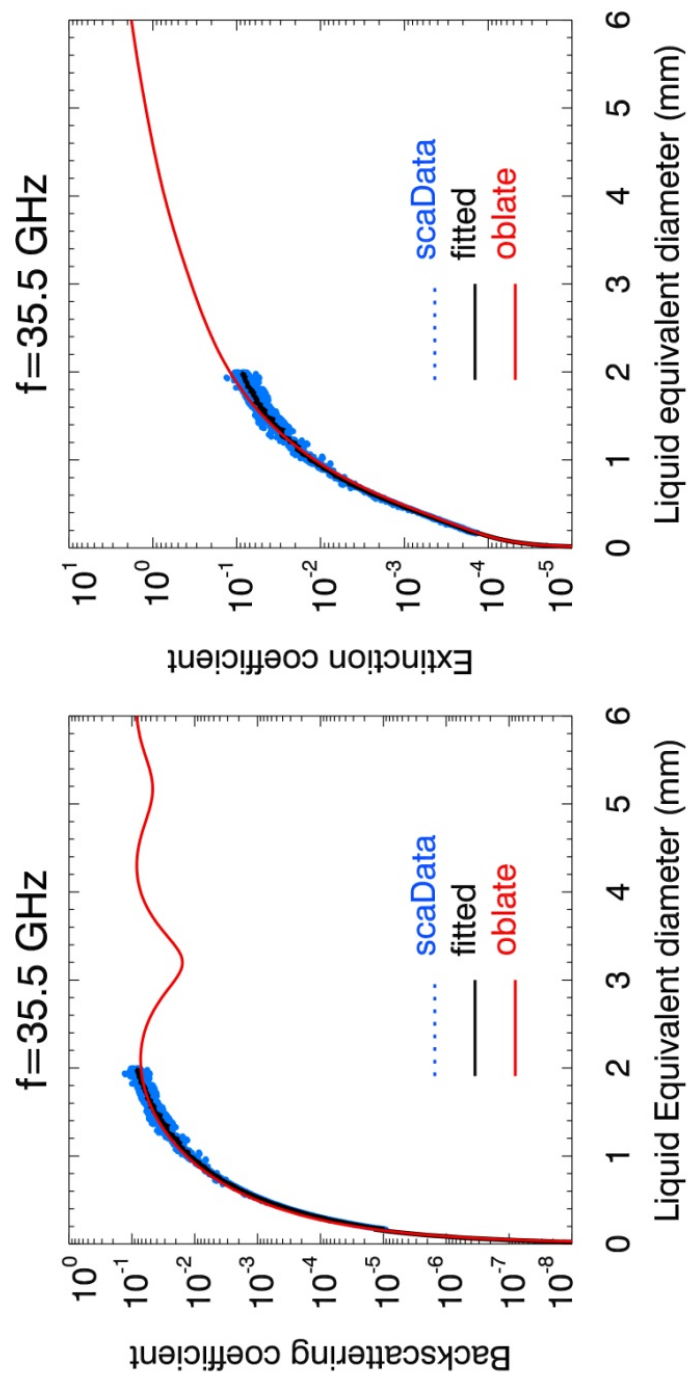
705

706

707

Fig.3 Backscattering (left) and extinction (right) coefficients from the scattering database (blue dots), simple scattering model (red curves), which is the randomly-oriented oblate spheroid with a constant effective density of 0.2 g/cm^3 and an aspect ratio of 0.7, and scattering-database-

708

709

710

711
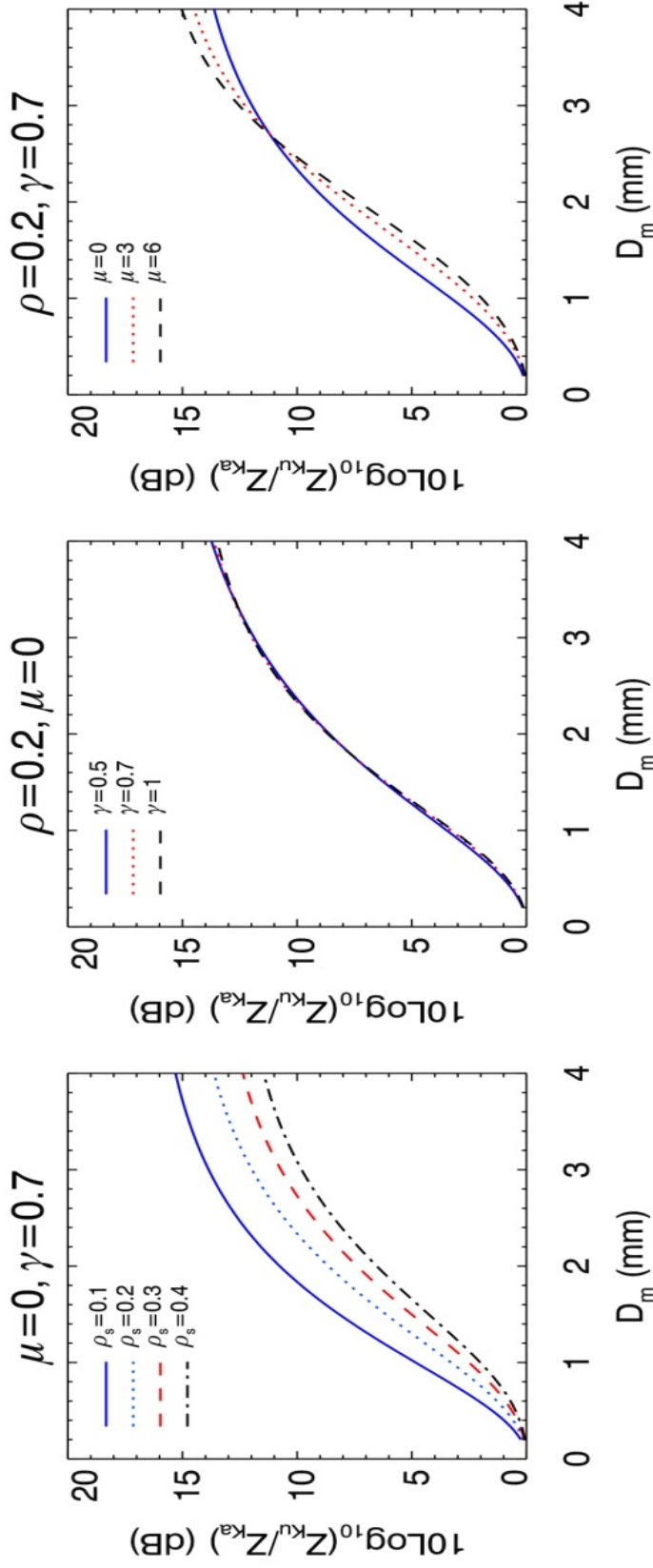
Fig.4 The differential frequency ratio (DFR=$10LOG_{10}(Z_{Ku}/Z_{Ka})$) as a function of equivalent-liquid median mass diameter D_m. (Left): DFR-D_m relations are plotted with several effective snow densities (ρ_s) from 0.1 to 0.4 g/cm^3 as the shape factor (μ) of the gamma PSD is set to zero and the aspect ratio (γ) of the oblate spheroid particles is set to 0.7. (Middle): DFR-D_m relations are plotted with the aspect ratios of 0.5, 0.7 and 1 at ρ_s=0.2 g/cm^3 and μ=0. (Right): DFR-D_m relations are plotted with the values of μ of 0, 3 and 6 at ρ_s=0.2 g/cm^3 and γ=0.7.
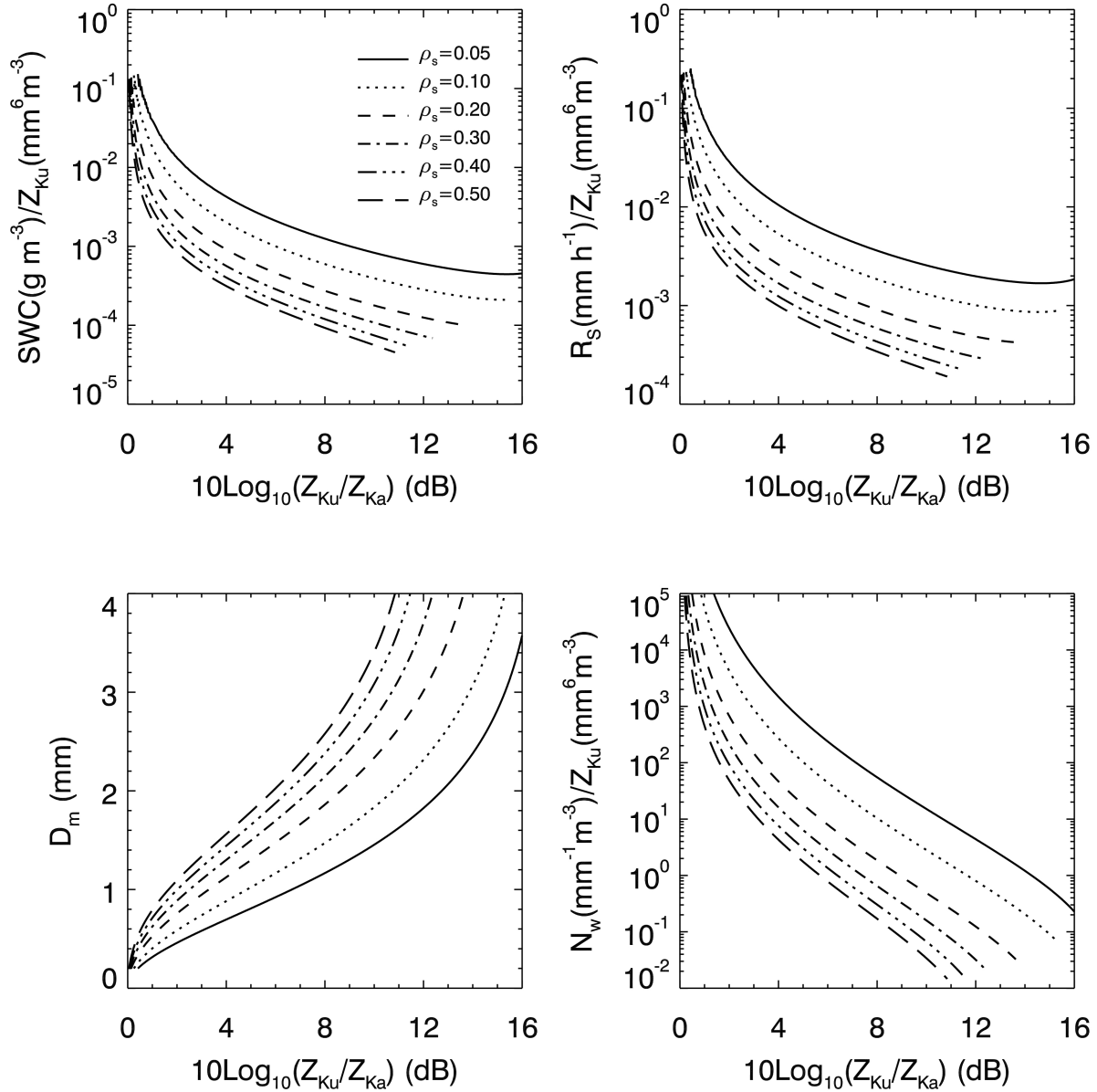
Fig.5 The retrieval look-up tables that show the snow water content (SWC) (top-left) and equivalent snowfall rate (R_S) (top-right), both of which are normalized by the Ku-band radar reflectivity factor (Z_{Ku}), as a function of the DFR, defined by $10LOG_{10}(Z_{Ku}/Z_{Ka})$, for several effective snow densities (ρ_s) with the values from 0.05 to 0.5 g/cm^3. The liquid equivalent median mass diameter D_m (bottom-left) and the PSD scale parameter N_w normalized by Z_{Ku} (bottom-right) are also plotted in terms of DFR.
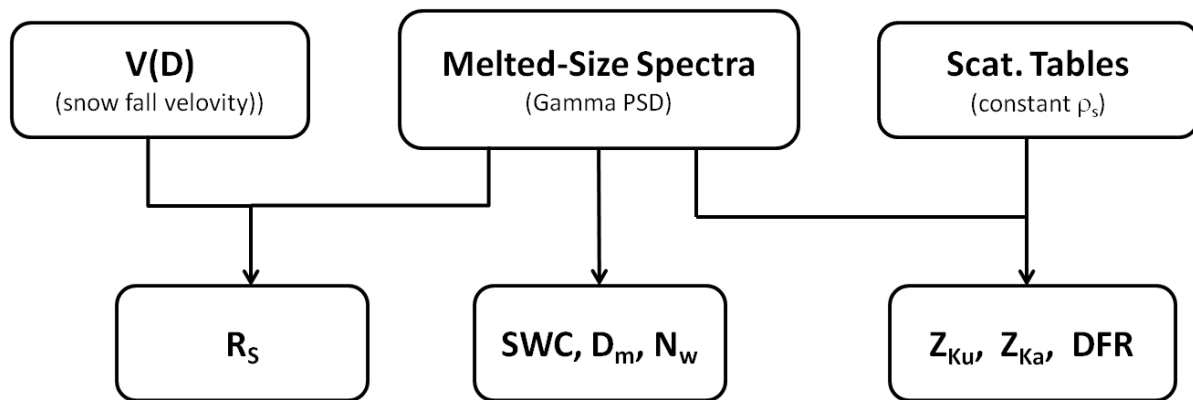
733

734

735 Fig.6 Flowchart of computing radar parameters and snow size and bulk properties.

736

737

738

739

740

741

742

743

744

745

746

747   Fig.7 The look-up tables used for the retrieval of SWC (left) and R_S (right) with μ of 0, 3 and 6,

748   respectively, as computed from the single scattering tables depicted in Figs.2-3.
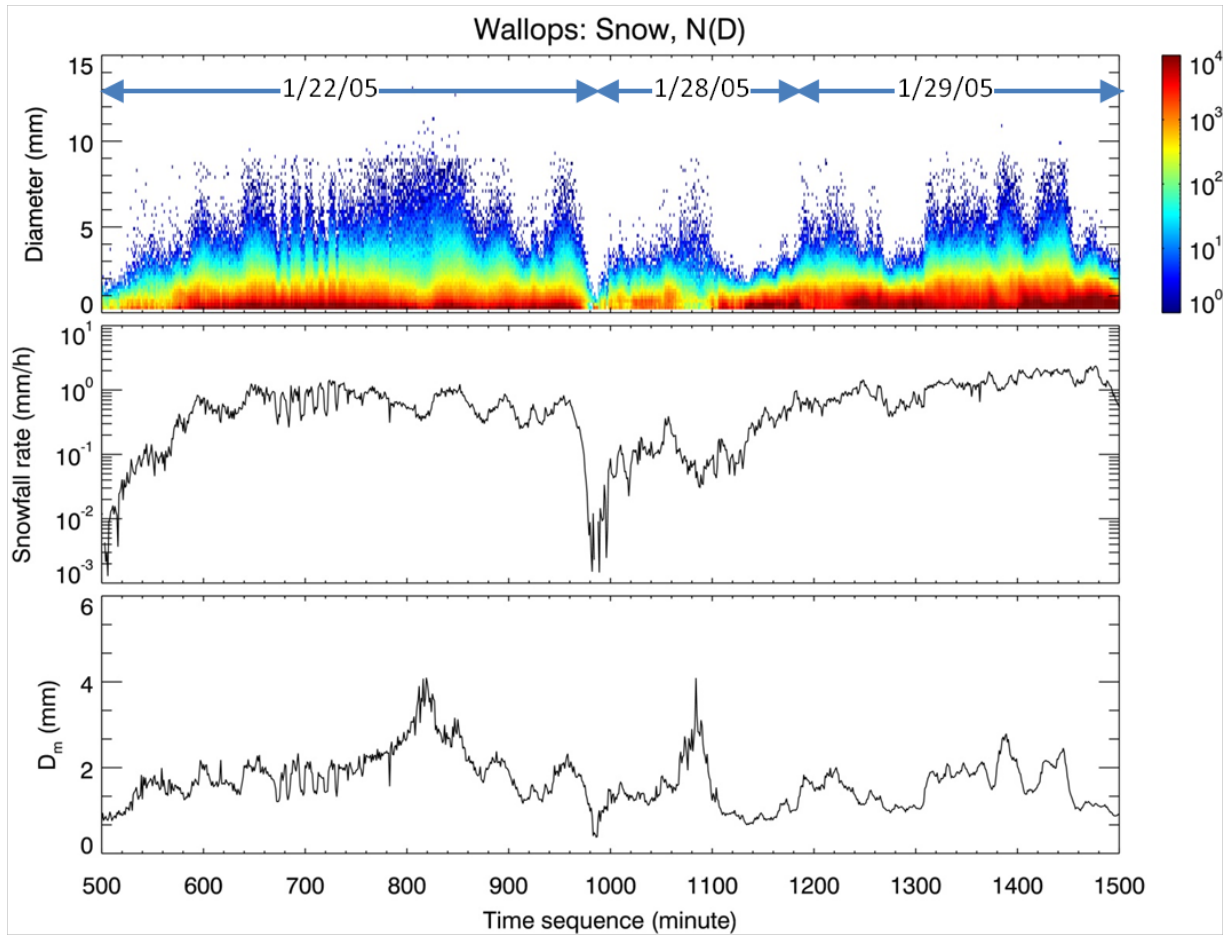
749
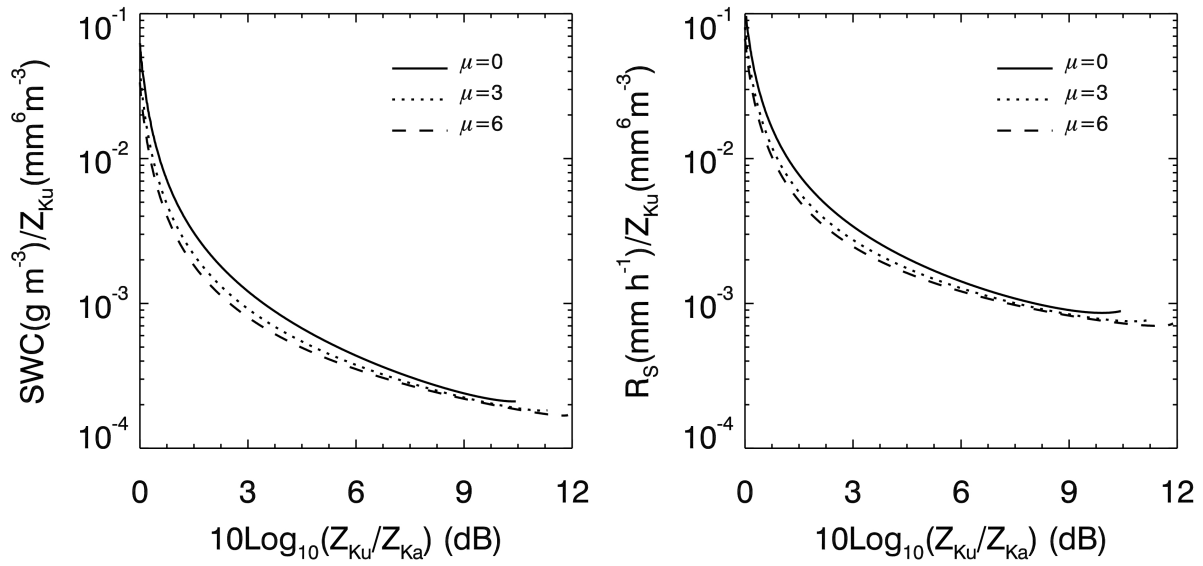
Fig.8 Example of a segment of the PSD data, obtained by averaging the measurements over 1-minute integration time, in time series taken from 8 snow events during winter of 2014 at the NASA Wallops Flight Facility using the SVI/PIP. The particle size spectra (mm^{-1} m^{-3}), shown in the color scale, are given in the top panel while equivalent snow fall rate and actual median mass diameter are displayed in the middle and bottom panels, respectively. The dates provided in the top panel correspond to the snow events displayed.
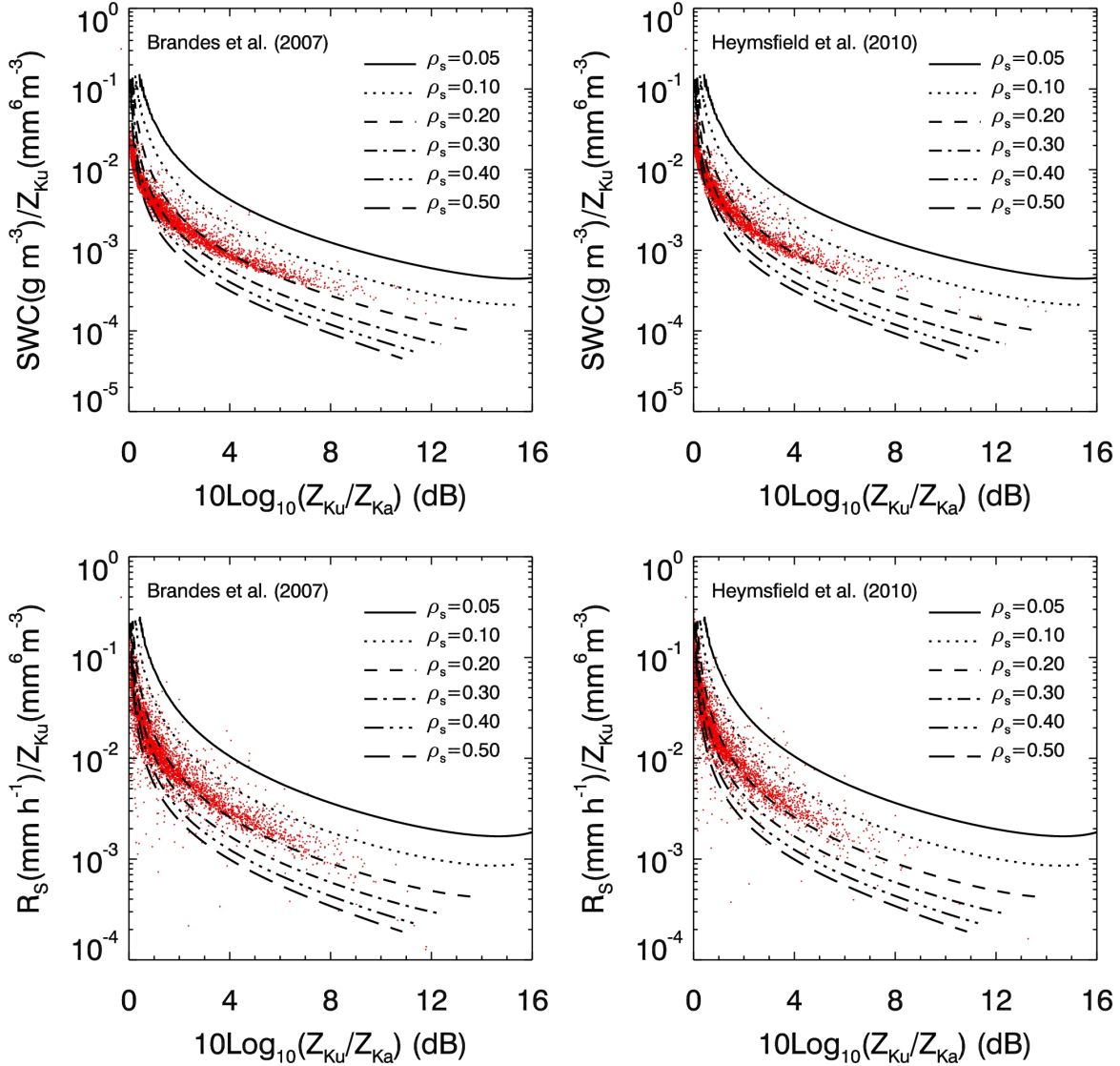
Fig.9 The snow water content (SWC) (top row) and equivalent snowfall rate (R_S) (bottom row), both of which are normalized by the Ku-band radar reflectivity factor (Z_{Ku}), as a function of the DFR, defined by $10LOG_{10}(Z_{Ku}/Z_{Ka})$, for several effective snow densities (ρ_s) with the values from 0.05 to 0.5 g/cm^3. The scatter plots (red dots) are the results derived from the measured PSD that were collected by the SVP/PIP from 8 snow events in the winter of 2014 at the NASA Wallops Flight Facility. Two empirical density-size relationships reported by Brandes et al. (2007) and Heymsfield et al. (2010) are used in converting the measured PSD to the snow mass spectra, and the results from their respective relations are shown in the left and right panels.
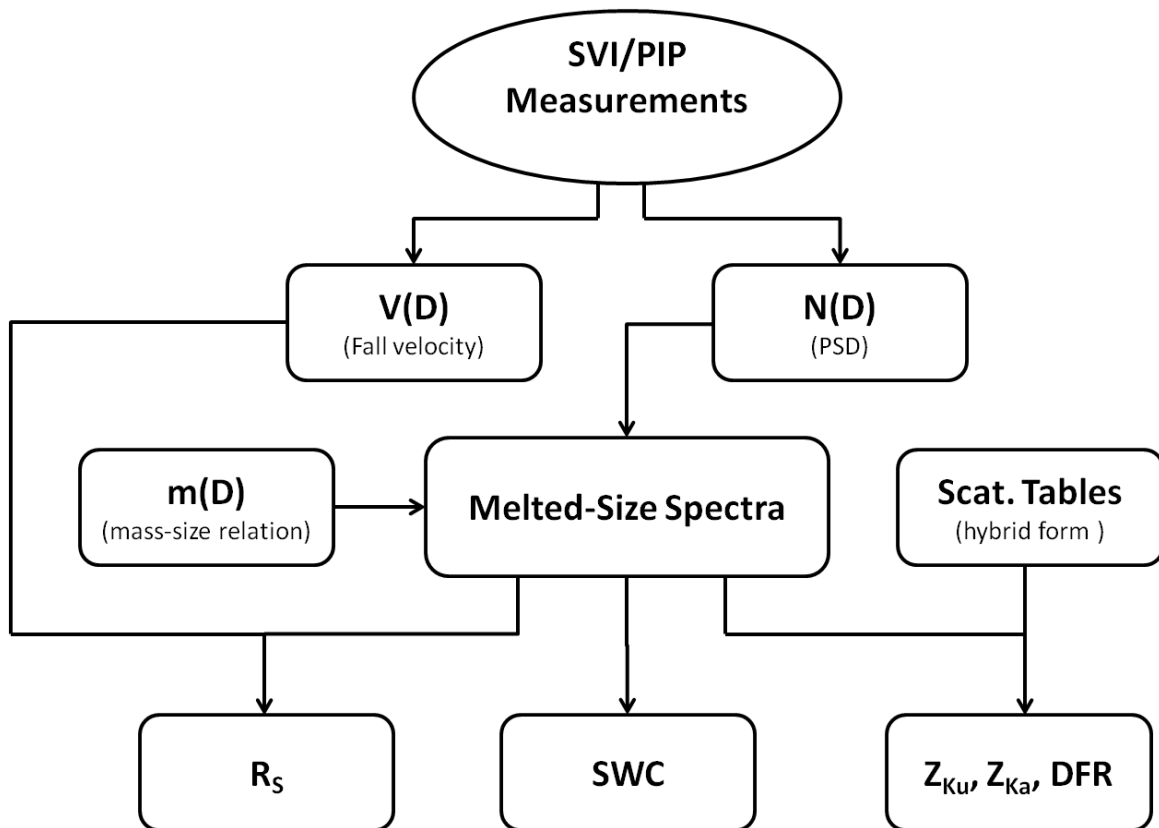
768

769

770   Fig.10 Flowchart detailing the procedures of obtaining radar reflectivities and snow parameters.

771